electronics

MDPI

Article

Investigation of Defect Formation in Monolithic Integrated GaP Islands on Si Nanotip Wafers

Ines Häusler [1], Rostislav Řepa [1,2], Adnan Hammud [3], Oliver Skibitzki [4] and Fariba Hatami [1,*]

[1] Department of Physics, Humboldt Universität zu Berlin, Newtonstrasse 15, 12489 Berlin, Germany; haeusler@physik.hu-berlin.de (I.H.)
[2] Institute of Physical Engineering, Brno University of Technology, Technická 2, 616 69 Brno, Czech Republic
[3] Department of Inorganic Chemistry, Fritz Haber Institute of the Max Planck Society, Faradayweg 4–6, 14195 Berlin, Germany
[4] IHP-Leibniz Institute for High Performance Microelectronics,15236 Frankfurt (Oder), Germany; skibitzki@ihp-microelectronics.com
* Correspondence: hatami@physik.hu-berlin.de

Abstract: The monolithic integration of gallium phosphide (GaP), with its green band gap, high refractive index, large optical non-linearity, and broad transmission range on silicon (Si) substrates, is crucial for Si-based optoelectronics and integrated photonics. However, material mismatches, including thermal expansion mismatch and polar/non-polar interfaces, cause defects such as stacking faults, microtwins, and anti-phase domains in GaP, adversely affecting its electronic properties. Our paper presents a structural and defect analysis using scanning transmission electron microscopy, high-resolution transmission electron microscopy, and scanning nanobeam electron diffraction of epitaxial GaP islands grown on Si nanotips embedded in SiO_2. The Si nanotips were fabricated on 200 mm n-type Si (001) wafers using a CMOS-compatible pilot line, and GaP islands were grown selectively on the tips via gas-source molecular-beam epitaxy. Two sets of samples were investigated: GaP islands nucleated on open Si nanotips and islands nucleated within self-organized nanocavities on top of the nanotips. Our results reveal that in both cases, the GaP islands align with the Si lattice without dislocations due to lattice mismatch. Defects in GaP islands are limited to microtwins and stacking faults. When GaP nucleates in the nanocavities, most defects are trapped, resulting in defect-free GaP islands. Our findings demonstrate an effective approach to mitigate defects in epitaxial GaP on Si nanotip wafers fabricated by CMOS-compatible processes.

Keywords: Si optoelectronics; monolithic integration; nanoheteroepitaxy

Citation: Häusler, I.; Řepa, R.; Hammud, A.; Skibitzki, O.; Hatami, F. Investigation of Defect Formation in Monolithic Integrated GaP Islands on Si Nanotip Wafers. *Electronics* **2024**, *13*, 2945. https://doi.org/10.3390/electronics13152945

Academic Editors: Elias Stathatos and Spyros N. Yannopoulos

Received: 20 June 2024
Revised: 23 July 2024
Accepted: 24 July 2024
Published: 26 July 2024

1. Introduction

The integration of gallium phosphide (GaP) on cost-effective silicon (Si) substrates is gaining significant attention. GaP is the most lattice-matched III–V semiconductor to Si, making it an ideal candidate for this integration. It features an indirect large band gap of approximately 2.3 eV, a high refractive index (n = 3.6 at 500 nm), significant optical non-linearity, and a broad transmission range from 0.55 to 11 µm. These properties make monolithically integrated GaP on Si highly suitable for various applications in optoelectronics and integrated photonics [1,2]. However, there are several challenges associated with the monolithic integration of GaP on Si, due to structural mismatch, thermal expansion mismatch, and interdiffusion. These material mismatches result in the formation of various defects in GaP, such as stacking faults (SFs), microtwins (MTs), and anti-phase domains (APDs), which strongly influence the electronic properties of GaP [3].

The small lattice mismatch of less than 0.4% at 300 K between GaP and silicon is still significant, and it limits the critical thickness of epitaxial GaP on Si to tens of nanometers [4]. Once this critical thickness is surpassed, the GaP layer experiences the emergence of threading defects, accompanied by the formation of misfit dislocations (MDs) at the

Si interface. Several distinct approaches have been applied to mitigate the misfit and significantly increase the critical thickness of the GaP epitaxial layer grown on Si, such as growth of $GaP_{1-x}N_x$ buffer that is lattice-matched to Si [5]. Additional strategies include selective-area growth (SAG) of GaP on pre-patterned nanostructured Si substrate [6,7], including nanoheteroepitaxy (NHE) where the growth confines on nanometer-sized Si tips embedded in SiO_2. The growth on Si nanotips creates key advantages, such as substrate compliance and migration of heteroepitaxial strain energy by dispersing it in three dimensions [8]. Consequently, it reduces the driving force for plastic relaxation and the formation of extended defects in the epitaxial layer. Moreover, the limited lateral extension of the Si tips facilitates the formation of single-step terraces on the Si seed area, contributing to a reduction in the antiphase domain density. The growth of GaP islands on Si nanotips using NHE has recently been reported [7].

In this paper, we present an extensive defect analysis of monolithic integrated GaP islands on Si nanotip wafers, delving into two sets of samples. The first group consists of GaP islands grown via conventional NHE on free and open Si tips [7]. The second group comprises structures grown using a modified NHE approach, where nucleation occurs in self-organized nanocavities formed on top of the Si tips. After these cavities are filled, the GaP islands emerge from them. The insets in Figure 1 schematically demonstrate the cross-sectional structures of both groups. Our results reveal that in both cases the GaP crystals are fully relaxed and align with the Si lattice. For both set of samples, defects are limited to a minimal presence of microtwins and stacking faults. Furthermore, for the second set, when GaP is nucleated in the cavities, most defects are trapped in the cavities, enabling the formation of fully defect-free GaP islands. Our findings demonstrate that the combination of NHE and self-organized nanocavities is an effective and scalable approach to suppress the formation of defects in epitaxial GaP islands integrated on Si nano-tips wafers fabricated by CMOS-compatible technology.

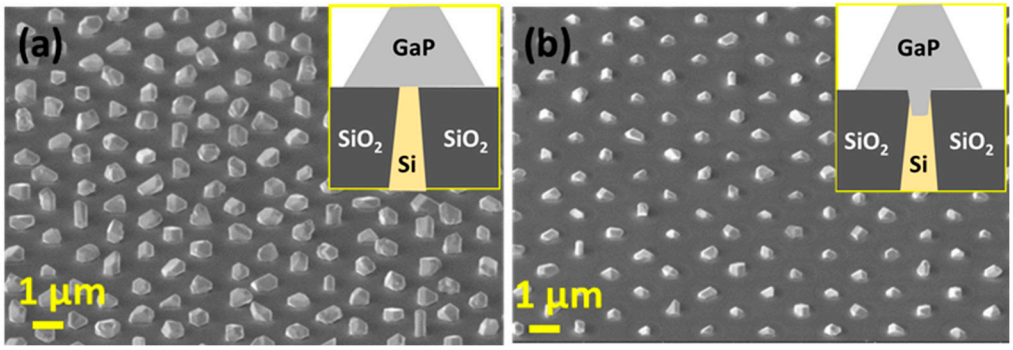

Figure 1. The tilted-view SEM images depict two GaP/Si samples grown under similar conditions. (**a**) GaP islands grown on open Si tips and (**b**) GaP islands on self-organized cavities atop the Si tips. In these SEM images, dark gray areas correspond to the SiO_2 mask, while the bright gray islands represent GaP. The insets show the cross-sectional schematic layout of a single island for both scenarios: islands grown on open Si tips (**a**) and islands protruding from the cavities (**b**).

2. Methods

The Si nanotip substrates were fabricated on 200 mm n-type Si (001) wafers in a state-of-the-art pilot-line running a 130 nm SiGe BiCMOS technology. The procedure of selective epitaxy of GaP islands on Si tips via NHE is discussed in detail by Kafi et al. [7]. In order to obtain the self-organized nanocavities in the SiO_2 film, the wafers were thermally annealed prior to growth at 800 °C. At this condition, Si at the top of the tip and surrounding SiO_2 react thermally, resulting in the volatile by-product SiO, and shortening the Si tips. In such a way, nanocavities were formed and the upper sides of the Si tips were confined in the SiO_2 [9]. The GaP structures were examined using scanning electron microscopy (SEM), scanning transmission electron microscopy (STEM), energy-dispersive X-ray spectroscopy

(EDXS), scanning nanobeam electron diffraction technique (SNBED), and high-resolution transmission electron microscopy (HRTEM).

In order to obtain detailed information on growth selectivity, material composition, and the defect formation of individual islands, the TEM samples were prepared using a ThermoFisher Helios NanoLab G3 FIB (Focused ion beam)-SEM DualBeam system (Thermo Fisher Scientific, Waltham, MA, USA), which provides gallium ions with energy up to 30 keV. The TEM lamellae were fabricated with the [110] orientation of the Si substrate, as a reference. To protect the GaP islands during the milling process, the surface was deposited with platinum (Pt) in a multi-step procedure using the electron beam induced deposition technique (EBID). We started the Pt deposition at high tilt angles to fill in the space between the GaP islands and the sample surface in order to minimize void formation and the resulting curtaining artifacts in the subsequent ion milling process. We finalized the preparation with low ion energy steps at 5 and 2 keV, respectively, minimizing the damage layer on the lamella side walls and achieving an estimated lamella thickness in the range of 25–40 nm at the region of interest.

Samples were analyzed with a TEM/STEM JEOL JEM2200FS (JEOL Ltd., Tokyo, Japan) at 200 kV. The instrument is equipped with a field emission gun, an ultrahigh-resolution pole piece (UHR), a Bruker LN2-free energy dispersive X-ray detector, one bright field and two dark field detectors, and a 1k slow-scan CCD camera from Gatan (Pleasanton, CA, USA). For the scanning nanobeam electron diffraction measurements (SNBED), the JEOL TEM was equipped with an ACOM/TEM (ASTAR) system (automated crystal orientation mapping with TEM) from the Nanomegas company (Brussels, Belgium).

3. Experimental Details and Results

Figure 1a,b present tilted-view SEM images of two samples grown under similar conditions (same growth rate, time, and temperature) using gas-source-MBE. In the SEM images, the dark gray areas correspond to the SiO_2 mask, while the bright gray islands represent GaP islands. The islands in Figure 1a are grown on open Si tips, whereas the islands in Figure 1b are nucleated in nanocavities. After these cavities are filled, the islands emerge from them. The insets provide schematic cross-sectional images of single islands for both scenarios. In both cases, the islands are grown selectively on the Si tips and there is no parasitic growth of GaP on the SiO_2 mask. It can be seen that the size and geometry of the islands are not uniform across the wafer, but they are distributed in similar morphological groups with predominated faceting in both cases. The islands grown on open Si tips (Figure 1a) are larger than the islands grown in the cavities (Figure 1b), which is a consequence of the materials used for the filling of the cavities.

Figure 2 shows the cross-section TEM images of an open Si tip (Figure 2(a.1)), a cavity on top of a tips (Figure 2(b.1)), and several islands grown on open tips (top images) and on the cavities (bottom images) after FIB-Lamella preparation.

The cross-sectional TEM images show that the islands vary in size and shape regardless of whether they were nucleated on open tips or within the cavities. However, once the cavities are filled, the shape of the GaP islands growing outside the cavities resembles that of the islands grown on the open tips. The islands in both cases can be classified into similar morphological and faceting groups. There are three dominant groups of islands: (I) symmetric shape with main facets along [111], as seen in #2, and #8 and #9; (II) islands mainly grown along [001], with [111] facets forming at advanced growth stages, such as #3 and #6; and (III) islands grown with combined facets and asymmetric shapes, such as #1, #5, #7, and #12. In addition to this observation, the cross-sectional TEM images preliminarily indicate that the islands grown on the cavities (Figure 2b) have fewer defects compared to those grown on the open tips (Figure 2a). This observation will be discussed in detail using further experiments.

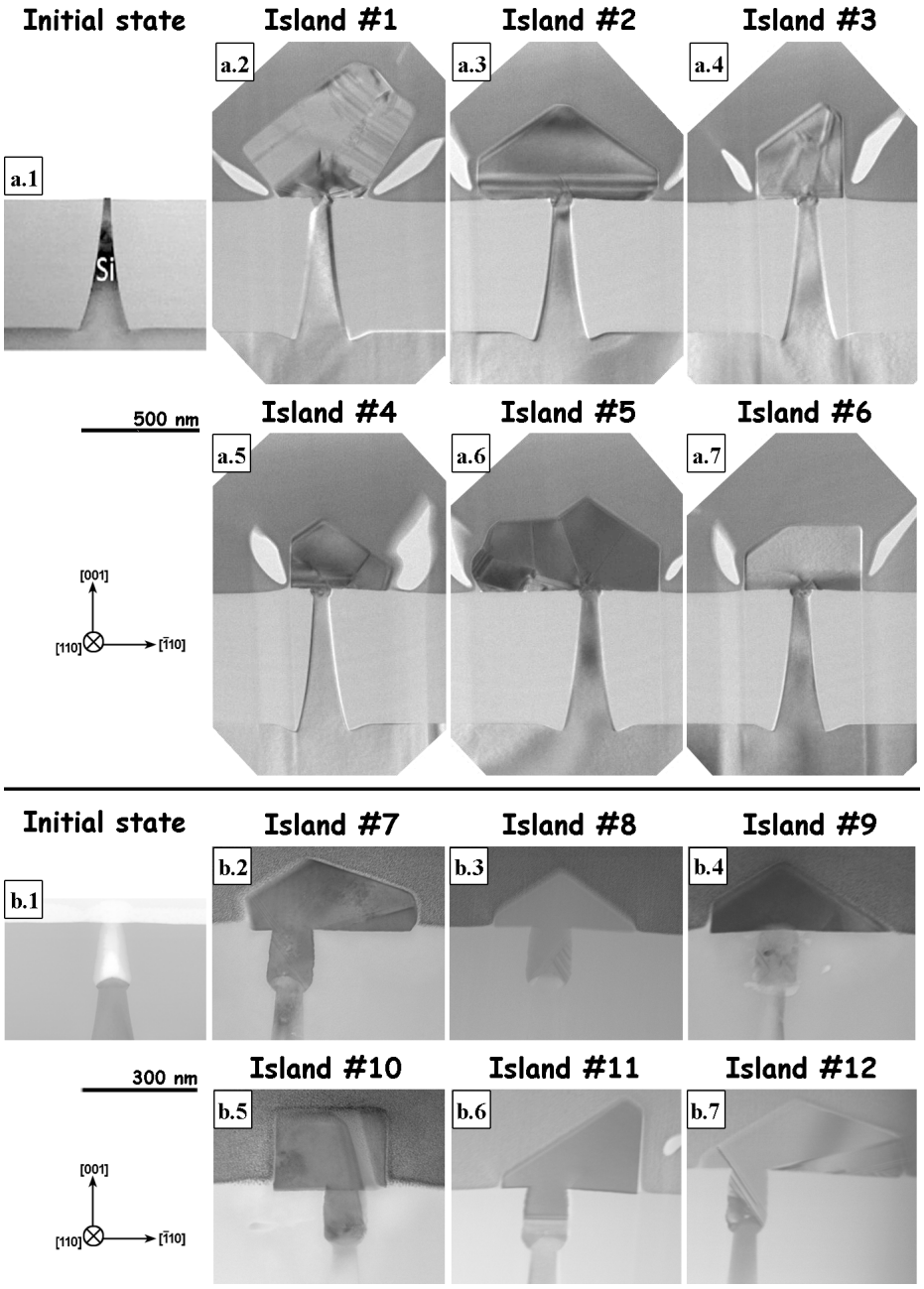

Figure 2. Cross-sectional TEM images of the Si tips and the GaP islands. (**a.1**) Open Si tips prior to GaP growth; (**a.2**–**a.7**) GaP islands grown on open Si tips; (**b.1**) Si tip with a cavity on top of that prior to GaP growth; and (**b.2**–**b.7**) GaP islands grown on the cavities.

First, we assess the selectivity of growth and the material composition of single islands using energy dispersive X-ray spectroscopy (EDXS). For the EDX elemental distribution map images, the sample regions were scanned with a beam diameter of 0.7 nm and the information was processed in Esprite software, version 1.9 to generate two-dimensional element distribution images. To eliminate the impact of morphology in the comparison of properties of islands grown on open tips and those grown in cavities, we specifically selected islands with similar morphology from both groups for our discussion. Figure 3 displays two islands with triangular cross-sectional shapes and a few facets (island #2, island #8), and Figure 4 exhibits two elongated islands with abundant facets (island #5, island #7). The bright-field STEM images of the islands are also shown on the left side of Figures 3(a.1,b.1) and 4(a.1,b.1).

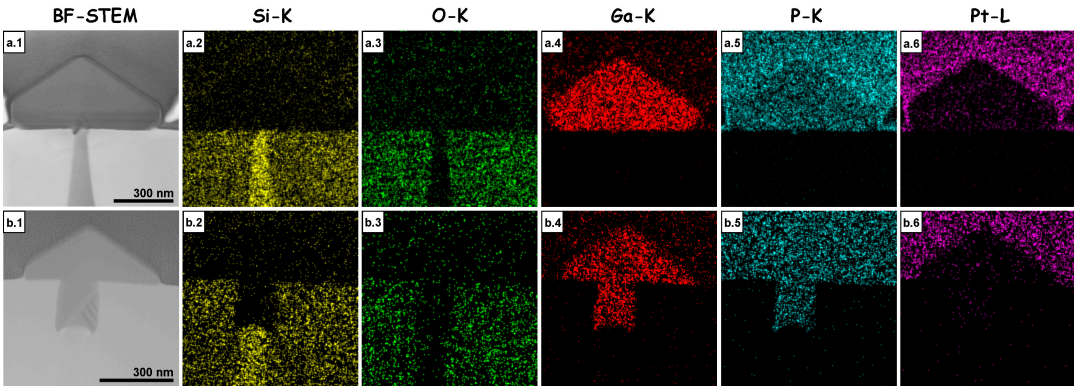

Figure 3. Exemplary element analysis using energy dispersive X-ray spectroscopy of island #2 and island #8 (Figure 2(a.3,b.3)). (**a.1**,**b.1**) are the Bright-Field STEM images from island #2 and island #8. The distribution maps for Silicon (**a.2**,**b.2**), Oxygen (**a.3**,**b.3**), Gallium (**a.4**,**b.4**), Phosphorus (**a.5**,**b.5**), and Platinum (**a.6**,**b.6**) are displayed using yellow, green, red, blue, and violet colors, respectively. The corresponding edges used for generating these maps are indicated next to each element's name above the maps.

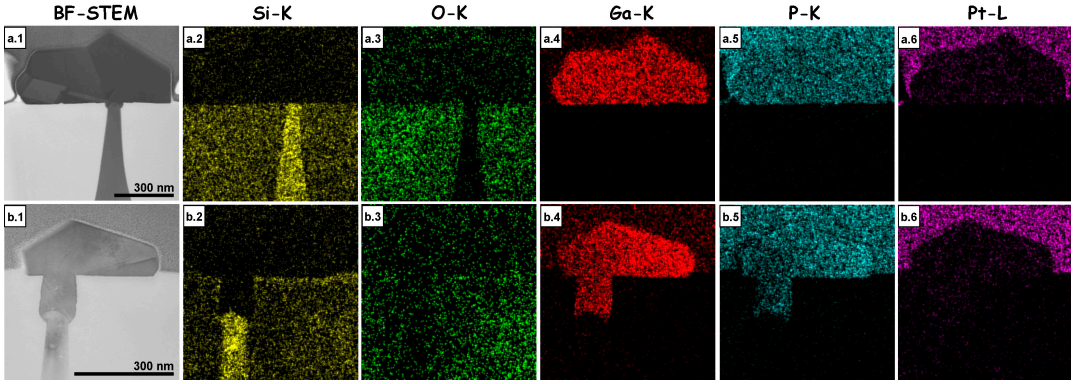

Figure 4. Exemplary element analysis using energy dispersive X-ray spectroscopy of island #5 and island #7 (Figure 2(a.6,b.2)). (**a.1**,**b.1**) are the Bright-Field STEM images from island #5 and island #7. The distribution maps for Silicon (**a.2**,**b.2**), Oxygen (**a.3**,**b.3**), Gallium (**a.4**,**b.4**), Phosphorus (**a.5**,**b.5**), and Platinum (**a.6**,**b.6**) are displayed using yellow, green, red, blue, and violet colors, respectively. The corresponding edges used for generating these maps are indicated next to each element's name above the maps.

The element distributions shown in Figures 3 and 4 confirm that the amorphous intermediate region consists of silicon and oxygen. The tip region consists of pure silicon (Figures 3(a.2,b.2) and 4(a.2,b.2)) and the island region grown on it consists of gallium (Figures 3(a.4,b.4) and 4(a.4,b.4)) and phosphorus (Figures 3(a.5,b.5) and 4(a.5,b.5)). A significant signal around the islands can be observed when we measure the phosphorus element distribution map. The reason for this is that the islands were covered by platinum during the FIB preparation. To generate the phosphorus element distribution map, we apply the P-Kα line at 2.010 keV with a peak width of 125 eV (representing 87% of the peak and ranging from 1.948 keV to 2.073 keV). However, the Pt-Mα edge at 2.05 keV closely overlaps with the P-Kα line, making it difficult to distinguish between the Pt protective layer surrounding the GaP islands and the phosphorus element distribution map (Figures 3(a.5,b.5) and 4(a.5,b.5)). To confirm that the area surrounding the islands exclusively contains platinum, an additional element distribution map was generated using the Pt-Lα edge at 9.435 keV (Figures 3(a.6,b.6) and 4(a.6,b.6)). The element distribution maps clearly prove the selectivity of the growth and that the islands are made purely of GaP, independent of the tip shape and the island morphology.

To gather insights into the crystal orientation and size of crystalline areas, the scanning nanobeam electron diffraction (SNBED) technique was performed. In this method, the designated area undergoes scanning with an electron beam, which is characterized by a very narrow beam with diameter in nanometers [10,11]. Unlike the convergent nature of the electron beam in conventional STEM mode, the electron beam in SNBED is nearly parallel, resulting in diffraction images with discrete reflections at each scanning point. The lateral resolution of the two-dimensional orientation and phase maps is determined by the selected beam diameter and step size. In our study, for the generation of the two-dimensional phase and orientation maps, a beam diameter of 1 nm and a step size of 3 nm were employed, ensuring no overlap between individual scan points. Figures 5 and 6 show the phase maps and orientation maps for the four islands presented in Figures 3 and 4.

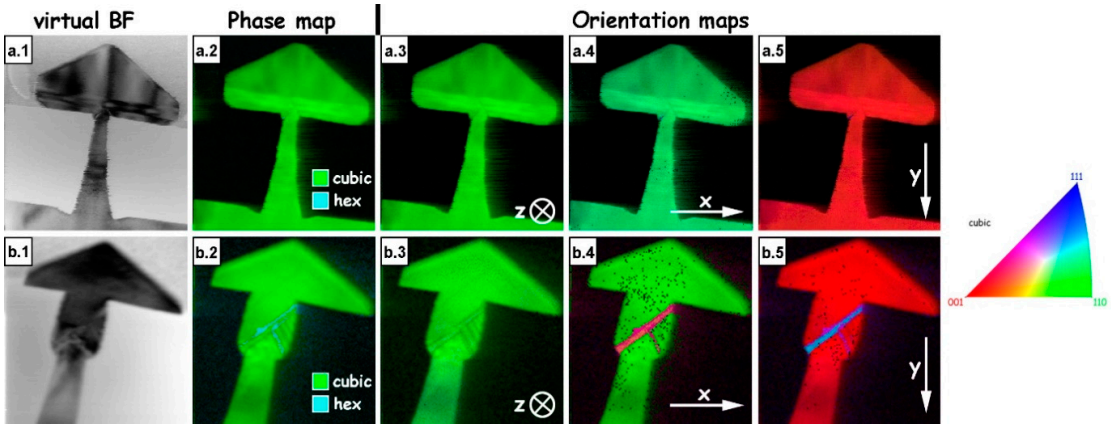

Figure 5. Analysis of phase and orientation using scanning nanobeam diffraction (SNBD) of island #2 and island #8 (Figure 2(a.3,b.3)). (**a.1**,**b.1**): Virtual Bright-Field STEM images from island #2 and island #8, respectively. (**a.2**,**b.2**): Corresponding phase maps of the islands. (**a.3**–**a.5**,**b.3**–**b.5**) show the orientation maps in three different directions. The color code on the right side represents the crystallographic direction of the cubic structures.

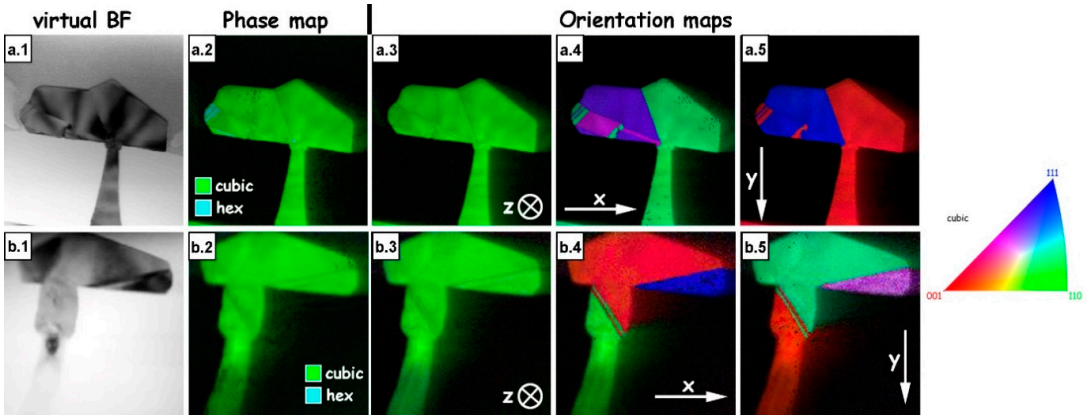

Figure 6. Analysis of phase and orientation using scanning nanobeam diffraction (SNBD) of island #5 (Figure 2(a.6)) and island #7 (Figure 2(b.2)). (**a.1**,**b.1**): Virtual Bright-Field STEM images from island #5 and island #7, respectively. (**a.2**,**b.2**): Corresponding phase maps of the islands. (**a.3**–**a.5**,**b.3**–**b.5**) show the orientation maps in three different directions. The color code on the right side represents the crystallographic direction of the cubic structures.

During the phase map creation process, the analysis routine encountered difficulty in distinguishing between cubic silicon and cubic GaP. This challenge arises from the comparison between simulated kinematic diffraction images and experimental dynamic diffraction images. In the kinematic scenario, the <110> diffraction patterns of silicon

(Fd-3m) and cubic GaP (F-43m) exhibit differences due to the presence of {002} reflexes. In Fd-3m, the {002} reflections are kinematically forbidden, while in F-43m, they are chemically sensitive. However, because the lamella thickness is less than the diameter of the Si tips, the {002} reflexes in Si are dynamically excited by indirect means (e.g., $(\bar{1}11)$ and $(1\bar{1}1)$), leading to their appearance in the diffraction pattern.

The analysis routine used for generating the phase image and orientation images only compares the positions of reflections, and not their intensities, with the kinematically calculated diffraction images. For this comparison, the required templates were generated based on the structural parameters listed in Table 1. Given the closely matching lattice parameters of silicon and cubic GaP (deviating by less than 0.4%), the routine cannot differentiate between cubic GaP and Si, and incorrectly selects GaP as the phase, as the GaP templates also incorporate {002} reflections.

Table 1. Structural parameters used for the analysis of diffraction images.

Structure	Space Group	Lattice Parameter	Atomic Positions				Ref.
GaP (cubic)	F-43m (216)	a = b = c = 5.450 Å	Ga:	0	0	0	mp-2490 [12]
			P:	0.75	0.25	0.75	
GaP (hex)	$P6_3mc$ (186)	a = b = 3.840 Å c = 6.330 Å	Ga:	0.667	0.333	0.500	mp-8882 [12]
			P:	0.667	0.333	0.874	
Si (cubic)	Fd-3m (227)	a = b = c = 5.44 Å	Si:	0.75	0.75	0.75	mp-149 [12]

The phase maps in Figures 5(a.2,b.2) and 6(a.2,b.2) contain blue marked areas in defect-rich regions, which may indicate a hexagonal phase. A detailed analysis of the diffraction patterns of the blue areas in the phase image also shows that this can be a superposition of two twisted <110> diffraction patterns of the cubic structure. This analysis confirms the existence of one or more twin boundaries. Additionally, based on our observations, no hexagonal phase was detected in the orientation maps. However, a detailed investigation of the defects and crystal structures in this area will be addressed later using HRTEM imaging.

A comparison between the islands nucleated on the open tips and those nucleated within the cavities reveals that the defect density within the islands on the cavities is significantly lower than in the islands on the open tips. In the former case, twins and other defects that initially arise during the transition from the Si tip to GaP are predominantly confined within the cavities and do not propagate into the actual island region.

It is noteworthy that all GaP islands observed in the z-orientation images exhibit a <110> orientation consistent with that of the silicon substrate. This suggests that the crystalline growth of the GaP islands is governed by the silicon tip, leading to epitaxial growth of GaP. This epitaxial relationship holds true regardless of the morphology of the islands.

To deepen our understanding of defect formation, we turned our attention to a defect-rich island (island #5, Figure 2(a.6)) and conducted a detailed investigation using HRTEM. Additional HR-TEM analyses of two other islands (island #7 and #8), which are have fewer defects, are provided in the Supplementary Materials. Figure 7a illustrates the cross-sectional TEM image of island #5, which was grown on an open Si tip. Our focus lies specifically on the GaP structures surrounding the Si tip, with precise analysis conducted in this area using high-resolution TEM imaging, as depicted in Figure 7b. The designated region of the GaP/Si interface, outlined by a yellow square in Figure 7b, served as the focal point for our investigation. This region is divided into five segments, separated by colored lines in Figure 7c. The transitions between these segments are identified by the presence of dislocations.

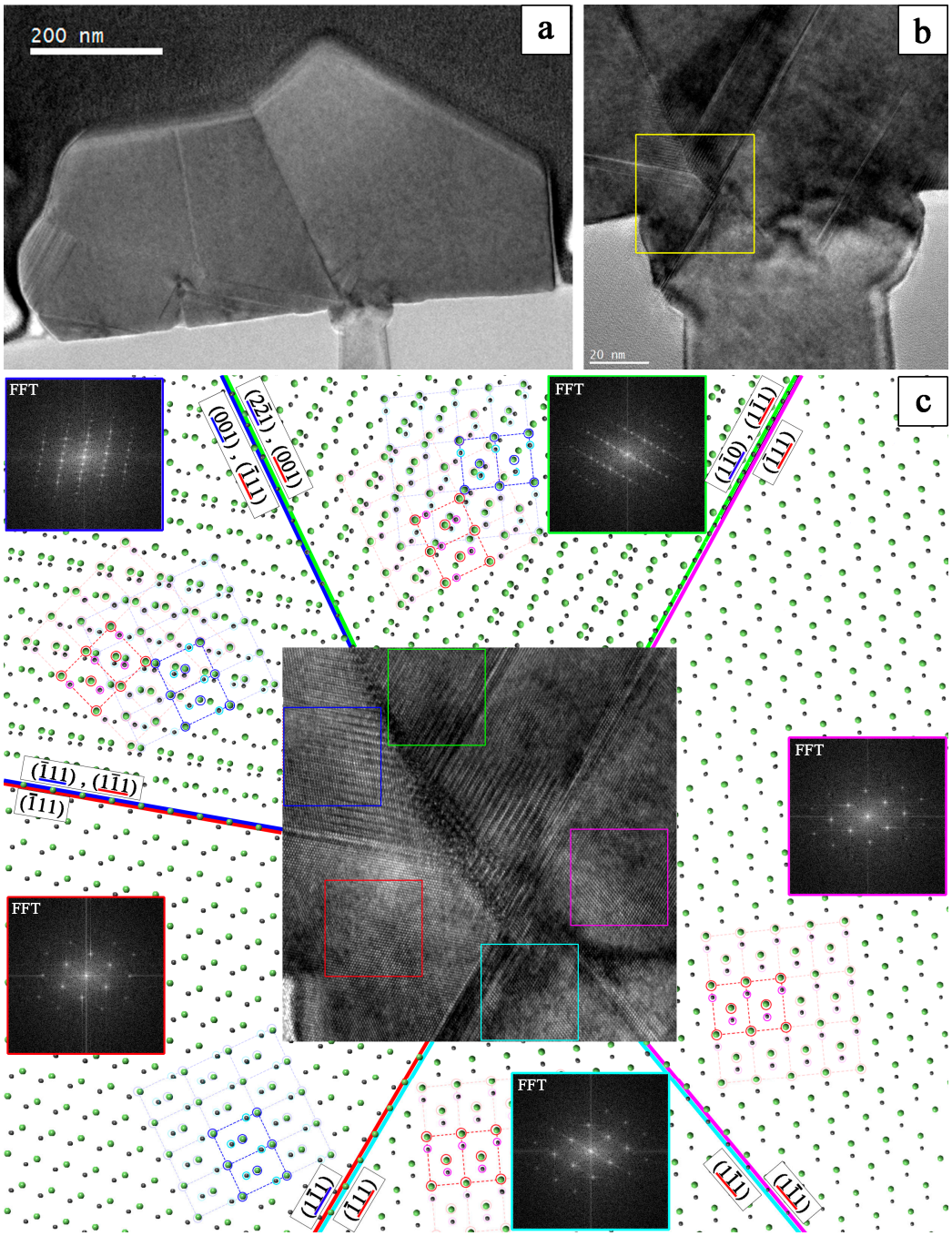

Figure 7. Structural analysis of an exemplary defect-rich island (island#5 in Figure 2). (**a**) Overview cross-sectional TEM image of the island. (**b**) High-resolution TEM of GaP structure around the Si tip. (**c**) Analysis of the HRTEM image of the area marked in the yellow square in part (**b**). The HRTEM image is divided into five segments, each separated by defect lines. From each segment, a representative area, delineated by colored squares, was selected for FFT analysis (see insets). Surrounding the HRTEM image are depictions of structures with their respective unit cells. A consistent cubic GaP structure with [110] orientation was observed across all areas. The crystallographic indexing of the interfaces between areas is shown. The unit cells for each crystallographic plane are drawn in the same color as the one used to underline the respective plane. The transitions of individual segments are dominated by stacking faults on the {111} planes.

Fast Fourier transformation (FFT) from each segment was performed on a representative region, delineated by colored squares (red, light blue, magenta, blue, and green), and

corresponding FFT patterns are presented in the insets of Figure 7c. Analysis of the FFTs from the red, light blue, and magenta segments revealed the presence of a single-crystalline cubic structure of GaP with [110] orientation. The structure, along with the positioning of its unit cell, is depicted in the surrounding area of the HRTEM image.

However, the analysis of the blue and green segments presented challenges due to the superposition of two twisted single-crystalline structures, induced by the sample thickness along the electron beam. This was evident from both Moiré patterns and a detailed FFT analysis. Comparison of the FFT patterns with simulated diffraction images of the hexagonal structure of GaP revealed no match; instead, a match was observed only with twisted cubic structures of GaP, arranged sequentially along the direction of the electron beam. The resulting structures, featuring twisted unit cells in their respective segments, are depicted in Figure 7c.

Thus, a consistent cubic GaP structure with [110] orientation was observed across all segments. The crystallographic plane indexing of interfaces between areas is marked by red and blue underlines, corresponding to the color-coded unit cells in Figure 7c. Transitions between segments are dominated by the presence of stacking faults on the {111} planes.

4. Discussion

In the heteroepitaxial growth of GaP on Si, antiphase domains (APDs) and strain induced by mismatch in coefficient of thermal expansion are key factors contributing to defect formation. APDs originate from the non-polar–polar interface, where growth dynamics leads to out-of-phase lattice occupation with gallium (Ga) and phosphorus (P). As APDs merge, they form antiphase boundaries (APBs). Several approaches exist to mitigate APDs during planar epitaxy of GaP on Si, such as growth of relaxed buffers [5]. However, patterning the Si substrate prior to growth, particularly through selective area growth that involves deposition of an oxide mask and pre-patterning of the Si substrate, has proven to be a valuable technique [3,6,7]. To understand the differences in defect formation between the investigated samples, we need to compare the growth dynamics and kinetics involved for both sets of samples: GaP islands grown on open Si tips and GaP islands on self-organized cavities atop the Si tips. In particular, the atomic-scale mechanisms of island growth, including the impact of different facets, need to be considered.

As discussed earlier, the nano-patterned Si tips on the substrate in NHE enable both vertical and lateral deformation, thereby distributing the mismatch strain in three dimensions. If mismatch dislocations form within the island, they can climb to an island edge. Additionally, due to the limited lateral extension of the Si tips, single-step terraces can form on the Si seed area, leading to a decrease in antiphase domain density. Thus, the defect density can be significantly reduced by combining the nanostructuring and substrate compliance, which is the capability to accommodate strain. The defect formation of the GaP grown on the open tips follows this scenario. In the second set of samples, GaP nanocrystals nucleate in self-organized cavities atop the Si tips, altering the NHE processes. The nucleation is similar to the Aspect Ratio Trapping (ART) technique, where patterned cavities are utilized to reduce defect formation during the monolithic integration of III–V semiconductors on Si [13–15].

ART is a modified approach to selective area growth and utilizes the epitaxial necking effect [13]. This effect traps the dislocations in a nucleation region, allowing for the growth of defect-free crystals above it. The epitaxial necking effect arises from crystallographic geometry and was first reported for the growth of GaAs on pre-patterned Si substrates [14], and later for other material systems, such as Ge/Si [15]. It was demonstrated that for the (001) interface, if the aspect ratio ($AR = h/l$) between the height (h) and length (l) of the predefined structures is sufficiently large, the first growth segment can confine the threading dislocations, preventing them from reaching the region above. Based on this principle, in the ART technique, cavities with a predefined high aspect ratio are fabricated prior to growth using patterned dielectric materials, such as SiO_2, on top of the semiconductor wafer. During growth, III–V materials are selectively deposited within these cavities.

To discuss the approach of ART in more detail, we consider the <110> {111} slip system as an example. This is a common case for epitaxial III–V layers on Si, where the threading dislocations lie in the {111} planes and are oriented along the <110> direction. If the wafer is (001) oriented and the cavities are aligned in the [110] direction (with a length of l and an oxide sidewall height of h, the projection of <110>-oriented dislocations lines onto the (110) plane will form an angle of approximately 55° with the [110] direction. If the aspect ratio of the cavity exceeds the tangent of 55°, which is about 1.4, the threading dislocations inclined to the [110] oxide sidewalls will be trapped within the cavity. To trap other threading segments besides those described by the <110> {111} slip system, the aspect ratio of the cavity must be designed such that the line direction of the dislocation projects into the oxide sidewalls.

As GaP nanocrystals grow, the defect trapping effect remains effective, and the epitaxial necking effect occurs. Specifically, during the nucleation of GaP in self-organized nanocavities, threading dislocations formed at the GaP/Si hetero-interface migrate to the SiO_2 sidewalls and can be trapped within the cavities. This results in dislocation-free GaP material above these traps. The cavities act as "trapping segments", as shown in Figures 5 and 6 for islands #7 and #8 (HR-TEM of these islands are provided in the Supplementary Materials). The dislocation lines form an angle of approximately 45° towards (001) plane, and the aspect ratio for both cavities is significantly higher than 1. This causes the dislocation lines to be fully projected into the oxide walls, resulting in the formation of defect-free islands emerging from the cavities. In the same way, other defects parallel to the cavity walls can be trapped.

The morphology of islands, whether during epitaxy on open Si tips or upon emergence from cavities, follows a similar pattern. As these islands grow, they develop more facets, reducing the surface area and minimizing the total surface energy. It is worth mentioning that one effective epitaxial strategy for controlling nanostructure shape and defect density involves manipulating the morphology of nucleation sites to favor specific crystallographic planes and facets. This approach relies on the principle that different crystal planes grow at different rates due to variations in surface energy [16]. In our study, the morphology of the GaP/Si interface, which is predominantly influenced by the shape of the Si tip and cavity, leads to similar growth dynamics and affects the orientation of defect lines within the GaP islands.

The stacking faults, as shown in Figure 7, predominantly occur on the {111} planes, often gliding along them. Facets play a crucial role akin to oxide walls; when the projection aligns, dislocations become trapped in small segments. These segments, negligible compared to the size of island, are illustrated in detail for facet- and defect-rich island #5. Consequently, even for large µm-sized islands, only a few defects emerge, and GaP grows as a single crystal while preserving its bulk properties.

5. Conclusions

To conclude, detailed structural investigations of individual GaP islands from samples integrated with CMOS-fabricated Si wafers and grown via NHE were conducted. Two sets of samples were examined: GaP islands nucleated on open Si tips and islands nucleated within self-organized nanocavities. In both cases, the GaP islands aligned with the Si lattice. The defects in the GaP islands were minimal, being primarily limited to microtwins and stacking faults. It was expected that the nanostructuring and substrate compliance in the NHE would significantly reduce defects. Our findings surpass this expectation, demonstrating that using self-organized nanocavities in NHE effectively traps defects within the cavities, resulting in fully defect-free islands.

These results provide compelling evidence of the successful elimination of defects in epitaxial GaP and demonstrate an effective and scalable approach to mitigating defects in epitaxial GaP on Si wafers fabricated using CMOS-compatible technology.

Supplementary Materials: The following supporting information can be downloaded at: https://www.mdpi.com/article/10.3390/electronics13152945/s1, Figure S1: High-resolution TEM of GaP islands #7 and #8. The first image on the left in the upper row shows the TEM image of the island. The squares indicate the areas where the high-resolution TEM was measured. The HR-TEM images are framed in the same color as the squares.

Author Contributions: Conceptualization, I.H. and F.H.; methodology, I.H., A.H., R.Ř., O.S. and F.H.; analysis, I.H.; writing—original draft preparation, I.H. and F.H.; writing—review and editing, A.H., R.Ř., O.S., I.H. and F.H.; supervision, F.H.; funding acquisition F.H. and O.S. All authors have read and agreed to the published version of the manuscript.

Funding: This research was funded by the German Research Foundation (DFG grant no: 428250328).

Data Availability Statement: Data will be made available on request.

Acknowledgments: The authors thank S. Kang for her support during MBE.

Conflicts of Interest: The authors declare no conflicts of interest. The funders had no role in the design of the study; in the collection, analyses, or interpretation of data; in the writing of the manuscript; or in the decision to publish the results.

References

1. Wilson, D.J.; Schneider, K.; Hönl, S.; Anderson, M.; Baumgartner, Y.; Czornomaz, L.; Kippenberg, T.J.; Seidler, P. Integrated gallium phosphide nonlinear photonics. *Nat. Photonics* **2020**, *14*, 57–62. [CrossRef]
2. Wang, Y.; Pan, Z.; Yan, Y.; Yang, Y.; Zhao, W.; Ding, N.; Tang, X.; Wu, P.; Zhao, Q.; Li, Y. A review of gallium phosphide nanophotonics towards omnipotent nonlinear devices. *Nanophotonics* **2024**. [CrossRef]
3. Park, J.-S.; Tang, M.; Chen, S.; Liu, H. Heteroepitaxial Growth of III–V Semiconductors on Silicon. *Crystals* **2020**, *10*, 1163. [CrossRef]
4. Soga, T.; Jimbo, T.; Umeno, M. Dislocation generation mechanisms for GaP on Si grown by metalorganic chemical vapor deposition. *Appl. Phys. Lett.* **1999**, *63*, 2543–2545. [CrossRef]
5. Bolshakov, A.D.; Fedorov, V.V.; Koval, O.Y.; Sapunov, G.A.; Sobolev, M.S.; Pirogov, E.V.; Kirilenko, D.A.; Mozharov, A.M.; Mukhin, I.S. Effective suppression of antiphase domains in GaP(N)/GaP heterostructures on Si(001). *Cryst. Growth Des.* **2019**, *19*, 4510–4520. [CrossRef]
6. Choi, W.; Huang, H.-C.; Fan, S.; Mohseni, P.K.; Lee, M.L.; Li, X. Selective area heteroepitaxy of p-i-n junction GaP nanopillar arrays on Si (111) by MOCVD. *IEEE J. Quantum Electron.* **2022**, *58*, 1–6. [CrossRef]
7. Kafi, N.; Kang, S.; Golz, C.; Rodrigues-Weisensee, A.; Persichetti, L.; Ryzhak, D.; Capellini, G.; Spirito, D.; Schmidbauer, M.; Kwasniewski, A.; et al. Selective Growth of GaP Crystals on CMOS-Compatible Si Nanotip Wafers by Gas Source Molecular Beam Epitaxy. *Cryst. Growth Des.* **2024**, *24*, 2724–2733. [CrossRef] [PubMed]
8. Zubia, D.; Hersee, S.D. Nanoheteroepitaxy: The Application of Nanostructuring and Substrate Compliance to the Heteroepitaxy of Mismatched Semiconductor Materials. *J. Appl. Phys.* **1999**, *85*, 6492. [CrossRef]
9. Kamath, A.; Skibitzki, O.; Spirito, D.; Dadgostar, S.; Mediavilla Martinez, I.; Schmidbauer, M.; Richter, C.; Kwasniewski, A.; Serrano, J.; Jimenez, J.; et al. Monolithic Integration of InP Nanowires with CMOS Fabricated Silicon Nanotips Wafer. *Phys. Rev. Mater.* **2023**, *7*, 103801. [CrossRef]
10. Rauch, E.F.; Veron, M. Coupled Microstructural Observations and Local Texture Measurements with an Automated Crystallographic Orientation Mapping Tool Attached to a TEM. *Mater. Sci. Eng. Technol.* **2005**, *36*, 552–556. [CrossRef]
11. Rauch, E.F.; Duft, A. Orientation Maps Derived from TEM Diffraction Patterns Collected with an External CCD Camera. *Mater. Sci. Forum* **2005**, *495–497*, 197–202. [CrossRef]
12. The Materials Project. Available online: https://next-gen.materialsproject.org (accessed on 1 April 2024).
13. Bai, J.; Park, J.-S.; Cheng, Z.; Curtin, M.; Adekore, B.; Carroll, M.; Lochtefeld, A.; Dudley, M. Study of the Defect Elimination Mechanisms in Aspect Ratio Trapping Ge Growth. *Appl. Phys. Lett.* **2007**, *90*, 101902. [CrossRef]
14. Fitzgerald, E.A.; Chand, N. Epitaxial Necking in GaAs Grown on Pre-Patterned Si Substrates. *J. Electron. Mater.* **1991**, *20*, 10. [CrossRef]
15. Langdo, T.A.; Leitz, C.W.; Currie, M.T.; Fitzgerald, E.A.; Lochtefeld, A.; Antoniadis, D.A. High Quality Ge on Si by Epitaxial Necking. *Appl. Phys. Lett.* **2000**, *76*, 3700. [CrossRef]
16. Zeng, H.; Yu, X.; Fonseka, H.A.; Boras, G.; Jurczak, P.; Wang, T.; Sanchez, A.M.; Liu, H. Preferred Growth Direction of III–V Nanowires on Differently Oriented Si Substrates. *Nanotechnology* **2020**, *31*, 475708. [CrossRef] [PubMed]